Summer 8-1-2015

Morphology-Property Relationship for Binary Organic Thin Films

Alyssa Lynn Griffin
University of Southern Mississippi

The University of Southern Mississippi

MORPHOLOGY-PROPERTY RELATIONSHIP FOR BINARY ORGANIC THIN FILMS

by

Alyssa Lynn Griffin

A Thesis
Submitted to the Graduate School
of The University of Southern Mississippi
in Partial Fulfillment of the Requirements
for the Degree of Master of Science

Approved:

_____
Dr. Song Guo, Committee Chair
Assistant Professor, Chemistry and Biochemistry

_____
Dr. Janice Paige, Committee Member
Associate Professor, Chemistry and Biochemistry

_____
Dr. Wujian Miao, Committee Member
Associate Professor, Chemistry and Biochemistry

_____
Dr. Karen S. Coats
Dean of the Graduate School

August 2015

ABSTRACT

MORPHOLOGY-PROPERTY RELATIONSHIP FOR

BINARY ORGANIC THIN FILMS

by Alyssa Lynn Griffin

August 2015

Organic thin films can be readily mass-produced through solution-based fabrication methods, including ink-printing and solution-casting because their light weight, flexibility, and inexpensive sources. Their applications range from organic field-effect transistors (OFET), organic solar cells (OSC), to organic light emitting diodes (OLEDs). Compared with pure component films, binary organic thin films (BOTF) allow for novel characteristics and specialized features to handle more demanding tasks. Due to the complex intermolecular interactions in BOTF, various microscopic phases with different morphological and electronic properties may be formed, and this information is difficult to extract through conventional bulk measurements.

This study focused on investigating the binary mixture of DH6T and PCBM thin films on HOPG through Atomic Force Microscopy (AFM) and Kelvin Probe Force Microscope (KPFM). Films of pure DH6T and pure PCBM and their mixture films were systematically analyzed to reveal topography and surface potential of different phases. This study found a vertical packing system of pure DH6T on HOPG surface in island forms. PCBM had a full coverage on the substrate with occasional pits which had been seen in previous studies. When adding different concentrations of PCBM to DH6T, the islands had changes in height as well as the presence of new morphology features that possibly consist of mostly PCBM. With this study, further analysis via annealings as well

as energy minimization simulations may deepen our understanding about molecular interactions of the DH6T/PCBM mixture at a microscopic scale.

ACKNOWLEDGMENTS

Firstly, a special thanks goes to my advisor Dr. Song Guo. This would not be possible without his patience and belief in my work. I would like to thank my other comitte members, Dr. Paige Buchanan, and Dr. Wujian Miao. Thier teaching and guidance are priceless and essential for my success. I would also like to thank Fredrick McFarland, my lab partner, who has taught me many new things from his experience in chemistry.

I would also like to thank the Department of Chemistry and Biochemistry. The department's faculty, staff, and students for encouraging me. They are part of my motivation to strive for success in research for the Department of Chemistry and Biochemistry as well as The University of Southern Mississippi.

TABLE OF CONTENTS

LIST OF TABLES

Table

LIST OF ILLUSTRATIONS

Figure

CHAPTER I

INTRODUCTION

Binary Organic Thin Film

Organic thin films provide a diversity of functions for new applications in technologies including organic field-effect transistors (OFETs)[1], organic photovoltaics (OPV)[2], and organic light emitting diodes (OLEDs).[3] Through a variety of solution-based processes such as spin-casting, drop-casting, dip-casting, and ink-printing[4], organic thin films can be readily fabricated.[5] Also, the resources needed to produce organic electronic devices are widely available, and production can potentially be very cost effective.

By using two organic components, binary organic thin films (BOTF) can provide some novel functions and properties that are urgently needed in the fast-growing field of organic electronics.[6] BOTFs have been applied into a variety of organic semiconductor devices. An example of BOTF used in solar cell research is P3HT/PCBM thin films.[7] Optical electronic devices are also incorporating BOTF to make light emitting diodes, which start to be commercially available in the forms of organic light-emitting diode (OLED) screens and lights.[8] This technology is widely used in TV, computer, and cellphone screens as well as concept cars and vehicles.[9] Compared with vacuum evaporation/sublimation methods, solution-based fabrication methods including ink-printing or solution-casting are able to mass-produce light weight, flexible, low-cost, and large-area devices. [10-15] With continuing research and developments, organic electronic devices, including BOTFs, may eventually replace their inorganic counterparts in many more applications.

There are a variety of intermolecular interactions to consider in a BOTF system. The two components will be called M_1 and M_2 as well as the substrate it will lay on, S. There will be interactions between M_1 - M_1, M_1 - M_2, M_2 - M_2, S - M_1, and S - M_2. The S, M_1, and M_2's interactions with the solvent during and after the drying process may also need to be included. At sub-molecular level, depending on the specific functional groups of the molecules, the intermolecular interactions may range from weak alkyl – alkyl to strong Coulomb interactions. These intermolecular interactions typically lead to various phases and domains in a BOTF system, whose sizes are generally in the nanometer – micrometer range.

The multiple phases formed in BOTFs may offer different optoelectronic and mechanic properties. The importance of morphology control at a micro-scale for organic electronic devices was summarized in an extensive review by Dang et. al. [16] It was noted that there are various parameters that can control the morphology of the polymer and fullerene mix. These parameters include the type of deposition of the film, solvents, ratio of donor to acceptor compounds, and annealing conditions. The morphology adjustment has a large impact on the performance of devices. The study of BOFT's local morphology can help to understand how the molecules are interacting and packing at nanoscale, which could help to design complex molecular mixtures with enhanced performances in the future.

AFM

Atomic Force Microscope (AFM) is a type of scanning probe microscope. A scanning probe microscope is different from an optical microscope because it uses a probe to raster-scan the sample surface in order to produce an image. Typically the tip is

attached to a cantilever that can be precisely moved three-dimensionally by a piezoelectric scanner on the AFM, as seen in Figure 1. In Atomic Force Microscopy measurements, interactions between the tip of the microscope's probe and the surface of the sample are being monitored to maintain the appropriate tip-sample distance. The surface's terrain can add force to the tip that will distort the cantilever's bending angle. The angle change of the cantilever is measured by the shift of laser beam reflected on the back of the cantilever into the photodiode detector. This change is recorded by the computer at each raster-scanning point, creating different z-axis data points. Local parameters, such as topography, surface potential, friction, magnetic properties, etc., can be measured depending on the type of tip and sample interaction analyzed.

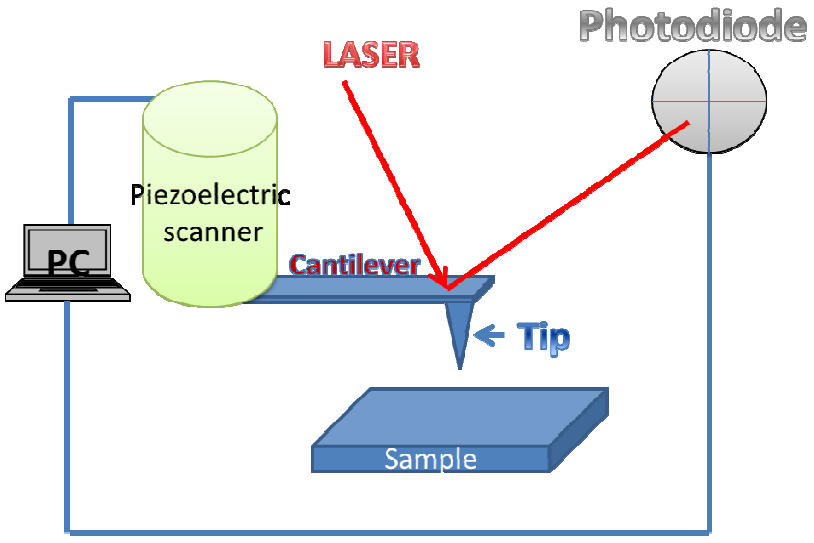

Figure 1. A basic AFM setup.

There are three basic modes of AFM: contact, non-contact, and semi-contact. These three different modes deal with different tip-sample interactions. In contact mode, the main interaction between the sample and the tip is the repulsive interactions or Pauli

repulsion interactions. Non-contact mode relies mainly on attractive Van der Waals forces.

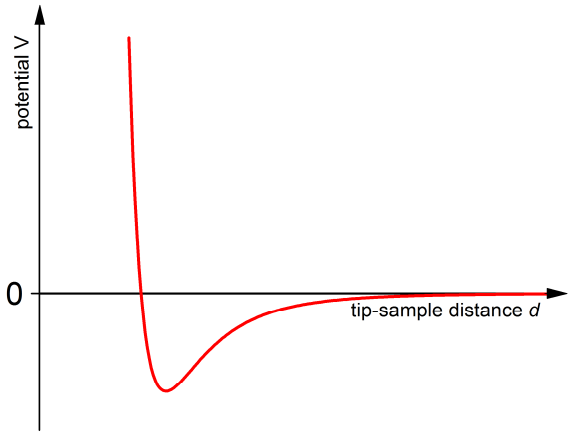

Figure 2. Van der Waals potential curve.

The mode of analysis used in this study is semi-contact topography AFM scan. Semi-contact mode works in the region between repulsive and attractive forces, as shown in Figure 2. In semi-contact mode, the cantilever is vibrated at its harmonic oscillation frequency. The oscillating tip would slowly come in contact with the surface, gently tapping the sample. As the tip comes closer with the surface, the oscillating tip is dampened because of the repulsive forces. The feedback system constantly adjusts the height of the scanning probe to maintain the amplitude of cantilever oscillation. By tracing the height of the scanner at each scanning point, the surface topography can be mapped.

Kelvin Probe Force Microscopy (KPFM) is another AFM mode used here. The most basic way that KPFM can be explained is its two-pass technique. The first pass is a semi-contact mode topography scan as explained before. The second scan will retrace the

topography from the first semi-contact mode scan and detect the electric surface potential. The purpose of the second tracing scan is to eliminate the contributions of the topography to the surface potential detection by keeping a constant tip-sample distance throughout the measurement.

KPFM can be explained in more depth by analyzing the energy levels of both tip and sample, as shown in Figure 3. The tip's work function is the difference from E_{Vac} and the Fermi level of the tip. The tip's Fermi level is denoted as φ_1. Similarly, the Fermi level of the sample is denoted as φ_2. In Figure 3 part (a), the tip did not make a connection with the sample. There are no electrons passing between the sample and the tip. There is a difference in their Fermi levels because their E_{Vac} are level. In Figure 3 part (b), the tip makes a connection with the sample. The difference in the Fermi levels between the tip and sample leads to electrons running from the sample to the tip until their new Fermi levels are equal. The result of this electron flow is that there are net positive charges on the sample and net negative charges on the tip, which leads to Coulomb interactions between the sample and tip. By applying a dc-voltage between tip and sample, the difference between their Fermi levels will be adjusted. When the dc-voltage equals the tip-sample work function difference, the vacuum levels will be realigned and all net charges will be reversed back, resulting to a total diminishing of the Coulomb interactions. In a two-pass KPFM experiment, the Coulomb interactions are closely monitored, while an external dc-voltage is systematically changed. The tip-sample work function difference would equal the external dc-voltage when there is no Coulomb interactions between the tip and sample.

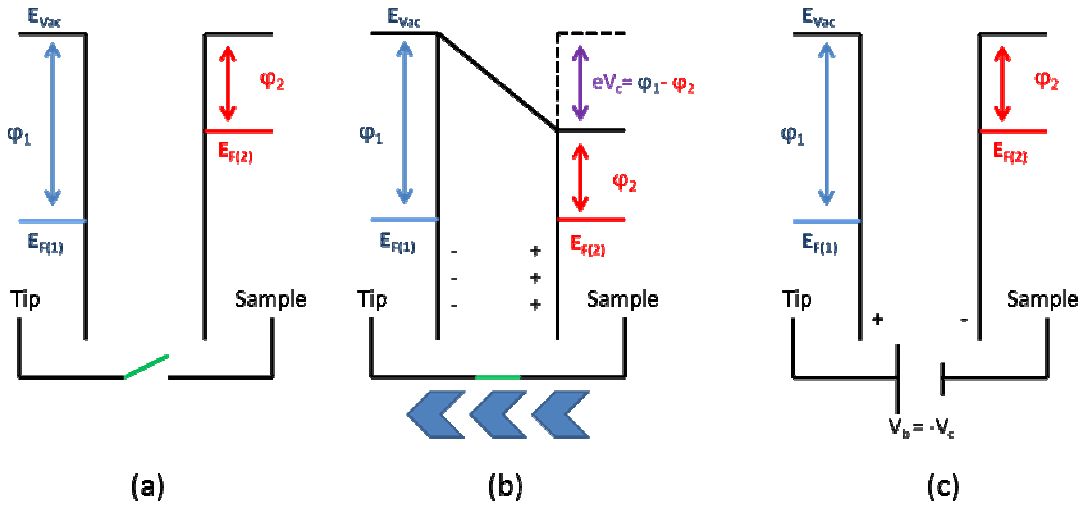

Figure 3. (a) The tip and sample are not connected, (b) the tip and sample are connected resulting in culmination of electrons, (c) dc-voltage is applied to realign the vacuum levels.

Atomic force microscopy (AFM), with its nanometer spatial resolution, is a very powerful method to probe the local phase and domain arrangements of organic thin films[17]. A (Dihexylsexithiophene) DH6T film was analyzed with AFM imaging and found to pack into features that looked like islands. There are a number of studies that show oligothiophene molecules aggregate into flat island-shaped features on a substrate.[5,8,18-21] Typically, these islands were scattered throughout the substrate and left the rest of the substrate uncovered, as seen in Figure 4.

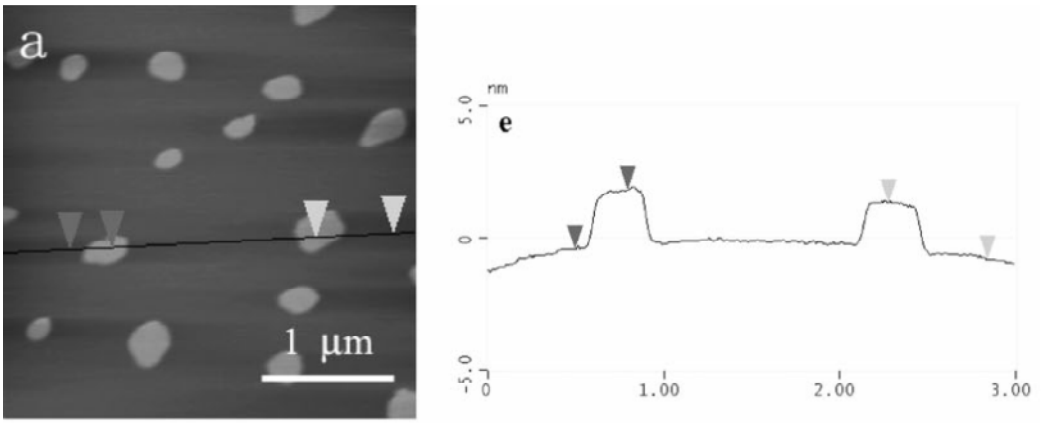

Figure 4. The image to the left is an AFM micrograph of DH6T islands on a mica substrate. To the right is a graph describing a cross section of the islands shown on the left. [22]

One of the more systematic studies done by Wang et. al. focused on DH6T aggregates' dependency on solvent choices and solution concentrations.[22] Their study showed that solvent polarity did not affect the morphology of the islands. Using different solvents, such as chloroform, THF, toluene, and benzene, to dissolve the DH6T and casting the resulting solutions on the mica substrate showed similar island morphologies. Their findings were informative and consistent to our initial findings. Another previous study stated that there is a correlation between the performances of the semiconductor to its thin film morphology. [5] These semi-conductive materials fall into the "donor-acceptor" systems in the OPV technology field today. Blending electron acceptors, such as fullerene derivatives, into conjugated polymers results in the formation of free charge carriers due to the charge-dissociation of photo-excited excitons. Thiophene rings in regioregular polythiophene molecules have an almost planar configuration. These planes of conjugated thiophene rings tend to stack in a "plane-on" configuration where the thiophenes are oriented parallel to each other. A similar but theoretical study by Duhm et. al. proposed probable packing models of the DH6T aggregates.[23] The impacts of P3HT's molecular weight on the morphological and photovoltaic properties of a binary mixture of

PCBM and P3HT were also investigated. [24] There is an optimal molar mass of the donor polymer that can provide the best photovoltaic parameters as well as the electro-optical properties. This specific molar mass likely leads to a preferred morphology for the polymer and fullerene active layers. Solvent also plays an important role in determining the morphology too. Zhang et al. varied the interface area between the domains of P3HT and PCBM by tuning the dichlorobenzene concentration in a solvent mixture and observed that the interfacial area has a positive effect on exciton dissociation between the two domains. [25] The effects of annealing were also studied by ultrafast time-resolved spectroscopy to show that post-annealed mixtures of PCBM and P3HT exhibit an increase in charge transfer and a reduction in recombination of excitons. [7]

Functioning thiophene with alkyl chains gives the molecule liquid crystalline properties.[26] Using AFM and XRD analysis, a high crystalline nature of the cruciform type oligothiophene dimers were found.[27] PCBM phase separation can enhance the thermal stability of the P3HT polymer network. [28] In a theoretical study by D'Avino et al., it was proposed that as the number of sexithiophene molecules increases on top of a layer of C_{60}, the sexithiophenes will change from a horizontal to a standing-up position.[29] The binary mixture of P3HT and PCBM in a semiconductor bulk heterojunction module has been tested to work for over one year in an outdoor environment without loss of performance.[30]

Research Aims

A typical polythiophene film has a film thickness of hundreds of nm. With a large amount of polymer molecules incorporated, this type of film is a very complex and challenging system to explore. A thiophene oligomer can be regarded as a model for P3HT, as well as other conjugated polythiophene molecules, by preserving the most important conjugated thiophene backbone motifs. In this study, using the smaller oligomer that is easier to understand and analyze is a better route to study the underlying molecular interactions. Decreasing the thickness of the film would expose more fractions of the molecules to surface analysis techniques, including AFM and KPFM. A theoretical study incorporated an octathiophene oligomer that has 8 thiophene units with PCBM and studied their energetically optimized molecular geometry.[31] Using density functional theory (DFT), the octathiophene oligomer was seen to bend over and to contour to the curvature of the PCBM. In the P3HT, the alkyl chains on the side also bent toward the curvature of the PCBM. In another theoretical study, it was observed that thiophene-like molecules tend to interact more with the fullerene side of PCBM than its butyric acid methyl ester tail.[32] These are some examples that theoretical calculations can analyze possible intermolecular interactions of the binary mixture. Li et. al. concluded that in a bulk heterojunction P3HT/PCBM, the PCBM will be lying flat in relation to P3HT.[33]

In this thesis, due to the complexity of polymer molecules, a BOTF of DH6T and PCBM is chosen as a model system. PCBM is known as an acceptor molecule and is widely used with different donor molecules because of its easy solubility and its fullerene characteristics. DH6T has high field-effect mobility, which peaks at $1 cm^2/V\ s$.[34] It was reported that OFET devices based on monolayer-thickness films of α,ω-DH6T can

exhibit hole mobility up to 0.032 cm^2/V s. Oligothiophenes and their alkyl- or styryl-substituted derivatives are stable in air because of their crystalline-like geometry and strong intermolecular interactions. It has been proposed that the functional units of conjugated polymers are actually small and rigid fractions of the polymer chain, which are composed of 5 – 10 repeating monomer units and called chromophores.[20] Due to the similarity of the thiophene backbones, DH6T can be regarded as a model molecule for the chromophore unit of polythiophene molecules.

There have been few studies on the morphology of DH6T and PCBM's mixture film. AFM is a less invasive microscopic technique that can give morphological data, and in the meantime KPFM can provide surface potential information. These two methods will be used synergistically to give experimental data to correlate with possible models of molecular packing. This study will approach film morphology analysis at a monolayer thickness to study the molecular aggregation and arrangements of the BOTF, which allow for easier correlation between experimental observations and possible molecular packing patterns. These studies can also give possible insights for morphological observations and molecular packing for more complex systems, such as a system involving polythiophene molecules. The research outcomes may be used as basic knowledge for further studies in similar semiconductive materials. This knowledge is important in improvements for organic semiconductors consisting of this type of binary mixture. Morphological knowledge, such as a donor-acceptor binary film with PCBM, can also help fine-tune its capabilities and control its electronic properties for specific uses. Also, film stability is another factor that the morphological observations can study. Information on enhancing the stability of an organic semiconductor will lead to better and more durable products.

These results could further accelerate the BOTF systems, including DH6T/PCBM and P3HT/PCBM, as a competitive material for future organic electronic applications.

CHAPTER II

HYPOTHESIS AND OBJECTIVES

Hypothesis

1. Rigid DH6T molecules may order in a staggered manner on HOPG due to π-π interactions between their sexithiophene backbones, allowing them to pack upright as islands. PCBM's greater variety of packing interactions will allow it to pack on HOPG more freely.

2. The packing of DH6T islands may be affected by the addition of PCBM due to PCBM's higher affinity to HOPG, changing the packing angle and topography of the DH6T islands.

3. The π-π interactions between DH6T and PCBM molecules could lead to different mixture phases that are preferred over the pure PCBM and pure DH6T phases on HOPG.

DH6T's sexithiophene backbones are known to be rigid and can be stacked with π-π interactions. This ordered packing could be expanded into island-like topographical features. Through previous studies of pure DH6T and pure PCBM films, respectively, it was known that PCBM has a higher bonding affinity to HOPG than DH6T does. With this understanding, it was hypothesized that the addition of PCBM would have an effect on the packing of DH6T islands. First, the interaction from PCBM can bend the sexithiophene backbone of DH6T and alter DH6T's packing angles on HOPG. Secondly, when the PCBM coverage increases, there could be new mixture phases of DH6T and PCBM due to the complex molecular interactions between the DH6T, PCBM, and HOPG. This would be consistent with previous literature reporting that a mixture of

thiophene and PCBM had an increase in stability than separated pure phases of thiophene and PCBM as a film. [28]

Primary Goal

The experimental goal is Investigation of morphology and electronic properties of DH6T/PCBM binary organic films through a combination of AFM measurements and modeling to understand the impact of intermolecular interactions on the molecular arrangements.

CHAPTER III

MATERIALS AND METHODS

Phenyl-C61-butyric acid methyl ester (PCBM) was purchased from American Dye Source Inc. with a purity of 99.5%. The dihexyl-sexithiophene (DH6T), chlorobenzene (99.7% purity), and chloroform anhydrous (99% purity) was purchased from Sigma Aldrich. All chemicals are used as is.

Phenyl-C_{61}-butyric acid methyl ester (PCBM) was dissolved in chlorobenzene, giving a concentration of 1.51 x 10^{-3} M. The concentration of dihexyl-sexithiophene (DH6T) solution in chlorobenzene was 1.47 x 10^{-3} M. Both solutions were slowly heated until all of the solids dissolved then cooled to ambient temperature before used as stock solutions to make other solutions. The sample solutions were all freshly made from stock solutions right before they were spin-casted. The films were prepared by spin-casting 10uL sample solutions on a freshly cleaved Highly Ordered Pyrolytic Graphite (HOPG) at 2000 RPM for 60 seconds.

Annealing studies allowed molecules to rearrange and repack with the help of solvent vapor, thermal energy, or both. A chamber was made for the annealing studies to place the films in for annealing. The chamber was a glass container with a Teflon lined cap as shown in Figure *5*. The film sample and a 2ml vial filled with chloroform were placed inside the chamber. The chamber was then placed inside an oven at a constant temperature of 70^{o}C for annealing. Once the annealing process was done, the sample was removed from the chamber to cool down and put in a sample holder to transport it to the AFM. Both semi-contact topographical and KPFM analysis were run on the samples.

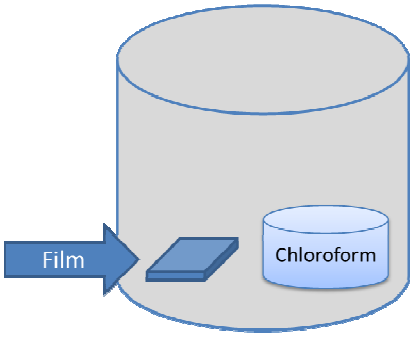

Figure 5. A basic setup of the annealing chamber.

Modeling of the DH6T and PCBM molecules and their aggregates were carried out on Spartan 14 software created by Wavefunction installed on a desktop computer (Quad-core CPU 3.4GHz, 8G memory). Molecules were drawn on ChemDraw Standard and uploaded into Spartan software. The energy is minimized using the (MMFF94) calculation. Minimization was checked multiple times to ensure consistency. For smaller sets of molecules, energy calculations at the ground state with Semi-Empirical (AM1) calculations were used.

CHAPTER IV

AFM AND KPFM RESULTS AND DISCUSSION

DH6T

Dihexlysexithiophene (DH6T) is a small molecule with a rigid sexithiophene backbone and two flexible alkyl chains attached to both ends of the conjugated thiophenes, as shown below in Figure 6. The sexithiophene backbone without the alkyl chains has a length range of 2.03±0.05 nm to 2.31±0.05 nm which was experimentally determined by Zotti et al. [35] A fully extended DH6T molecule has a theoretical length of 3.65 nm.[36] DH6T is shown to have reasonable solubility in chlorobenzene. As discussed in introduction, DH6T molecules can aggregate due to strong intermolecular interactions between their sexithiophene backbones.

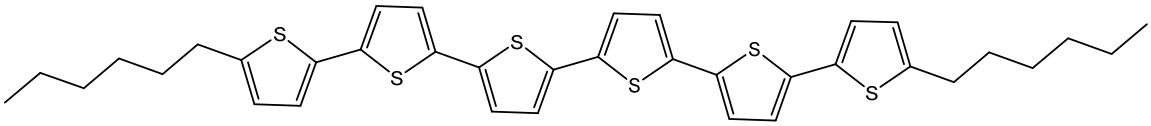

Figure 6. Scheme of one DH6T molecule.

In order to make a thin film and observe it, highly ordered pyrolitic graphite (HOPG) was used as a substrate for the DH6T to be spin-casted on. The resulting thin film was then analyzed using Atomic Force Microscopy (AFM). The topography mode of AFM works by gently scanning the surface of the film while receiving electrical feedback that creates a 3-D mapping of the surface it scans. HOPG is a relatively flat surface that can be easily cleaved with a piece scotch tape. When HOPG was scanned by AFM, the resulting micrograph showed distinct features to the surface of HOPG. Cleaving HOPG with scotch tape did not leave a perfectly flat graphite surface. In a large scale, HOPG has a slight waviness that can be seen in a topographical image such as Figure 7. The surface

will also have what is commonly described as step edges and terraces of graphite layers. In Figure 7, the HOPG surface is shown with DH6T aggregates.

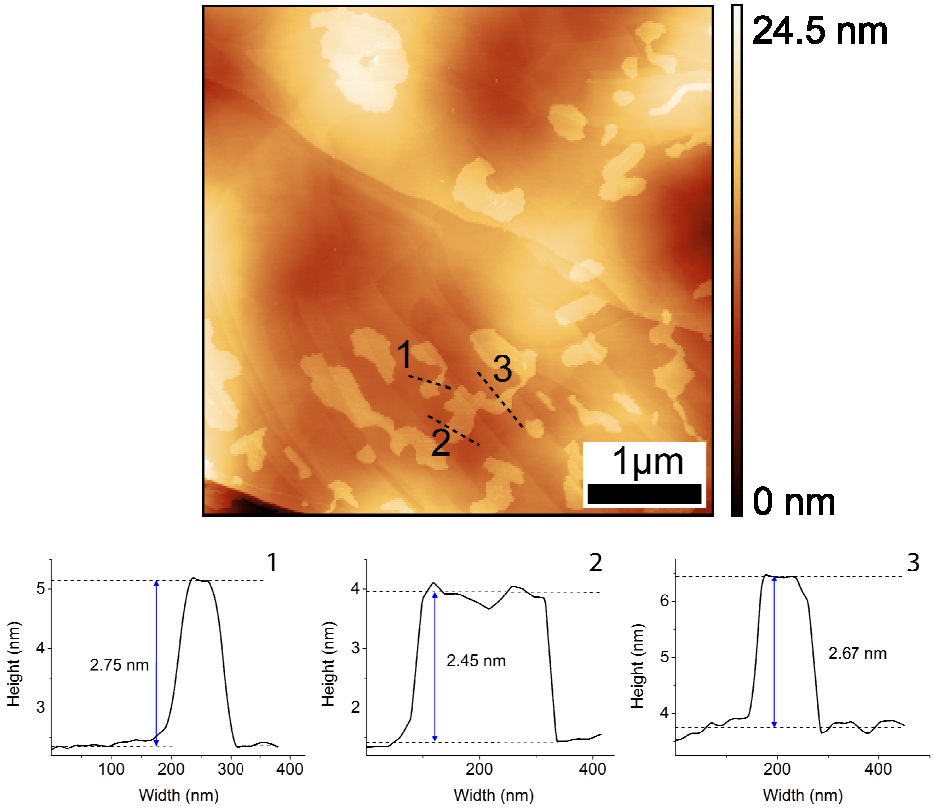

Figure 7. Top left is a 5×5 µm topographical AFM image of DH6T on HOPG. The bottom graphs from left to right correlate to the cross-sections marked in the topographical image. Each cross section shows a height averaging at 2.60 nm for the islands.

The features of the DH6T film seen were islands throughout the scanned image. These islands vary in shapes and sizes. The crossections over the islands are shown in the bottom graphs of Figure 7. As seen in the figure, DH6T has a consistent island height, averaging at about 2.6 nm. These crossections also showed that the islands have a flat surface at the top. Figure 8 shows a closer view of the DH6T film as well as HOPG's flat terraces and step edges. The step edges did not interfere with the continuity of the island

heights. Also there was a clearer view of the even height of the island on one flat terrace of HOPG.

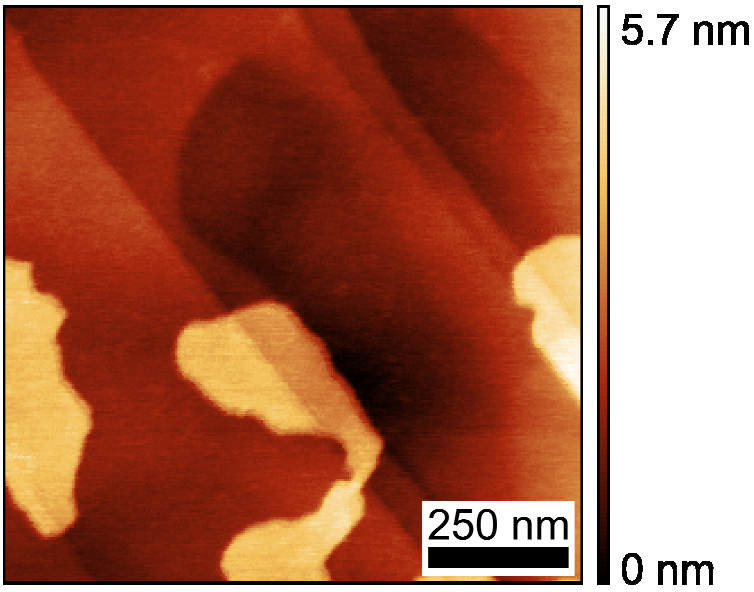

Figure 8. 1×1 nm topographical AFM image of DH6T on HOPG. This image is a close up of the area around the first cross section of Figure 1.The image shows a close up of the DH6T islands over bare HOPG.

In literature, similar features were found by depositing a DH6T film on a different substrate. Wang et al. developed DH6T films on mica and observed uniform plate-like features in AFM micrograms,[22] similar to our DH6T micrograms such as in Figure 7. They also collected a height of 2.4±0.2 for their DH6T islands and explained the heights by a model with the molecules packing at a 45^{o} angle to the substrate.

Our results lead into a study of different possible molecular packing models using the program Spartan 10. The models were studied for their lowest energy conformation by comparing relative energies to each other. Figure 9 shows the most stable conformation of a DH6T molecule in vacuum.

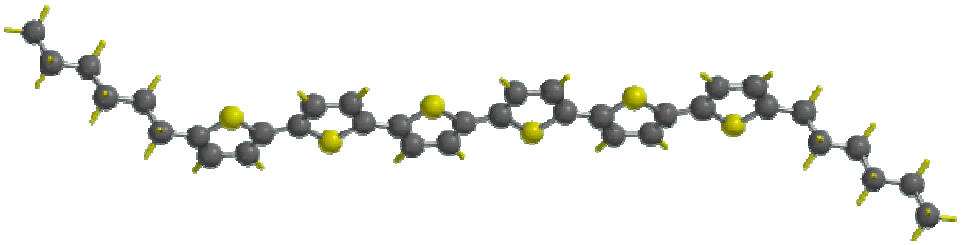

Figure 9. A scheme of one DH6T modeled with Spartan 10 showing a linear sexithiophene backbone with two flexible alkyl chains bent in different directions.

It was apparent that the DH6T modecule was not a perfectly straight rod at its lowest energy conformation. Although the sexithiophene backbone was straight and does not bend or twist into another conformation, the alkyl chains prefered to bend opposite of each other. This bending gave the molecule a zigzag orientation that shortened the overall length of the DH6T. Figure 10 displays the molecular stacking of two DH6T molecules. The rigid sexithiophene backbones lined up back to back with each other with the thiophene rings line up in the model. This interaction between the conjugated rings is known as π-π intermolecular interactions. The distances between the thiophene rings in the sexithiophene backbones of the two DH6T molecules were set at values from 0.5 Å to 5.5 Å with 0.5 Å increments, and their relative energies were calculated. The most stable distance between the two DH6T backbones was 4 Å throughout the whole sexithiophene backbone chain.

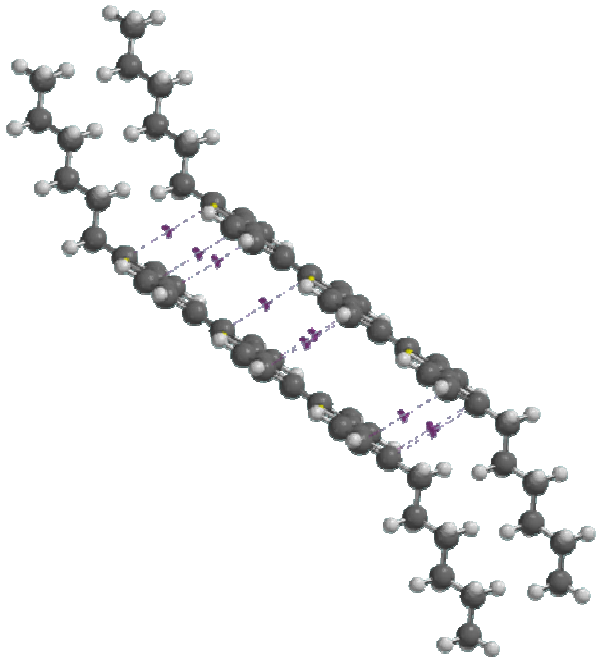

Figure 10. A scheme of two DH6T molecules aligned in a staggered formation.

When a layer of graphene, as a representive of the HOPG substrate, was added to the modeling system, an approximate topographical height of the aggregates could be deduced. The DH6T molecules were tilting on the substrate, showing a max height of about 2.73 nm in Figure 11. It is reasonable to expect that the intermolecular π-π interactions can continue to stack more DH6T molecules and eventually form 2-D islands.

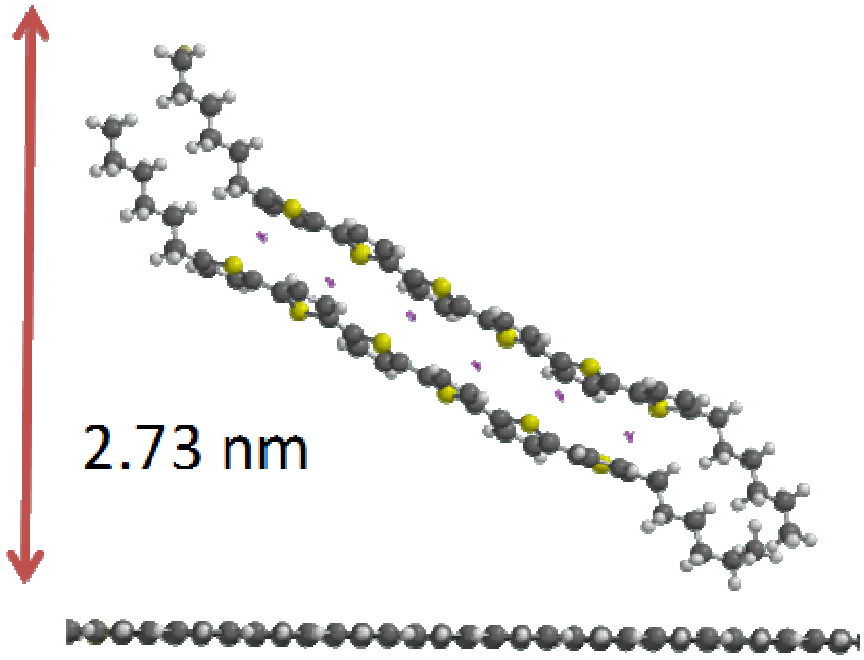

Figure 11. Two DH6T molecules aggregated on graphene.The height of this model is 2.73 nm.

The π-π stacking models of thiophenes were thoughouly explained in Yamagata et al.'s studies on octothiophenes.[37] They measured the theoretical HOMO and LUMO levels of the octothiophenes in relation to the position of the neighboring molecules. Their studies was done with their thiophene rods spacing set at 3.8 Å, which is close to the stable distance shown in our studies. These π-π interactions were the driving force for self assembly with alignments of the conjugated rings. Hlawacek and Teichert's topical review supported the "island clusters" model by showing that the bigger the cluster size, the more prone the linear DH6T will assemble in a vertical position.[8] This trend can be seen in Figure 12, which compares the binding energy to how many thiophene backbones are packed together. As seen in the figure, the top models with the blue line represent the vertical assembly while the bottom models with the red line represent the horizontally

assembling molecules. There is a point (cluster size of ~ 20 molecular) where the vertically assembled molecules have a larger binding energy per molecule. Considering the islands observed in our experimental results are likely composed of thousands of molecules, the standing model proposed here is consistent with both our experimental and modeling results.[8]

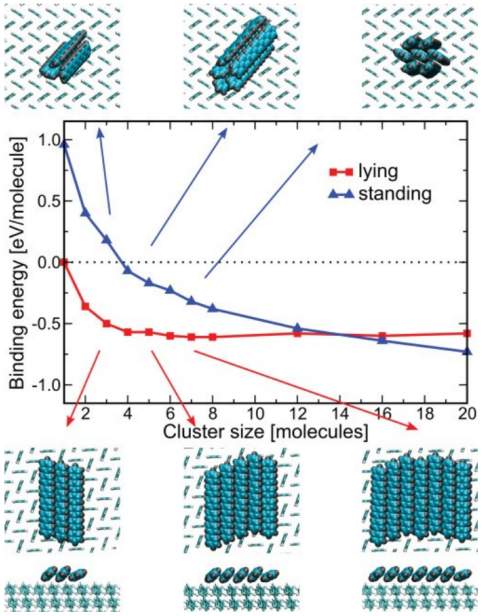

Figure 12. 6P cluster packing in the horizontal orientation as seen on the bottom and their relative binding energy per molecule as graphed as the red line. The vertical packed molecules are shown at the top of the graph and their binding energies are plotted by the blue line. [8]

PCBM

Phenyl-C_{61}-butyric acid methyl ester (PCBM) is a functionalized C_{60} fullerene molecule with improved solubility. PCBM has a size of around 1 nm and is a good electron donor. PCBM's added groups that make up the PCBM "tail" is key in PCBM's greater solubility in relation to fullerene. The enhanced solubility makes it feasible to

prepare PCBM thin films via a solution-based method, and one example image of the PCBM thin film on HOPG is shown in Figure 13.

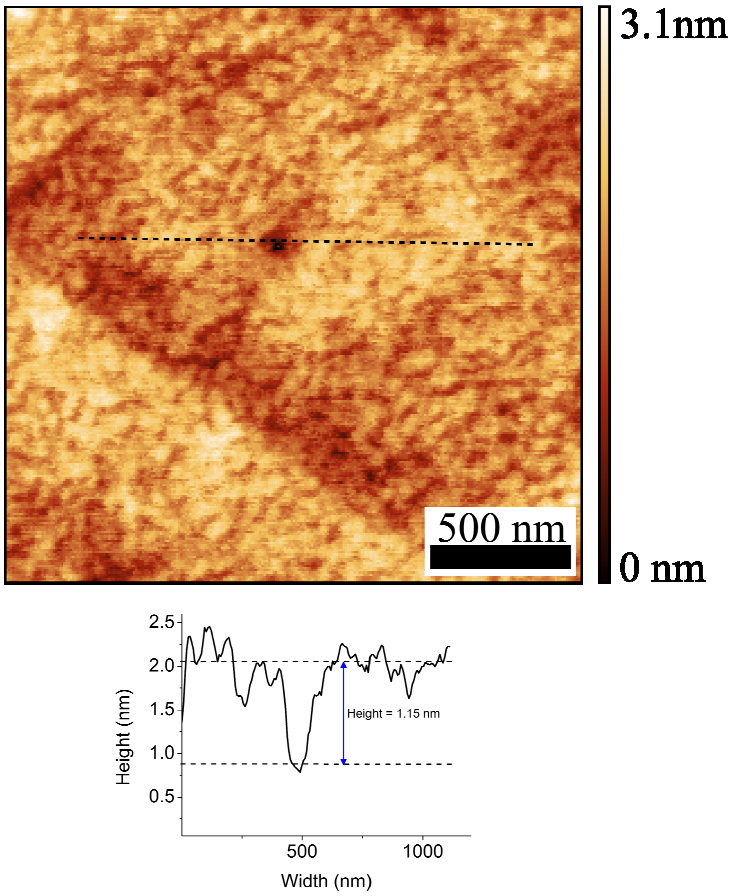

Figure 13. 2×2 µm microgram of a PCBM film over HOPG

Unlike the DH6T film, the graphite features were harder to see on this sample of a PCBM film on HOPG. PCBM fully covered the substrate probably because of its higher affinity to graphite than DH6T. There was a pit in the middle of this microgram, whose depth was 1.15 nm, consistent with the height of a PCBM monolayer (~ 1 nm). A recent communication from Guiseppe Paterno et al. showed that solvent choices have an effect on PCBM's crystallization properties.[38] With chlorobenzene, PCBM was revealed experimentally through x- ray diffraction to form crystals in a triangular shape with a

triclinic unit cell dimensions of a = 1.383 nm, b = 1.592 nm, and c = 1.908 nm. The tail of the PCBM was movable although its bulkiness would have steric interferences that give less freedom of movement than a simple alkyl chain attached to the fullerene.

Our experimental results were within reason of the literature results gathered in the AFM analysis. The film's surface in the AFM's analysis showed a relatively flat surface on a micron scale with sub-micron pits scattered throughout the film. The high coverage of PCBM on HOPG was not surprising as high van der Waals binding energies between fullerenes and the graphite surface were reported.[39]

15% Mixture

A 15% PCBM in DH6T solu tion in chlorobenzene had a PCBM concentration of 1.5×10^{-4} M and a DH6T concentration of 9.8×10^{-4} M. This mixture was spin-casted on a HOPG substrate and imaged as seen in Figure 14.

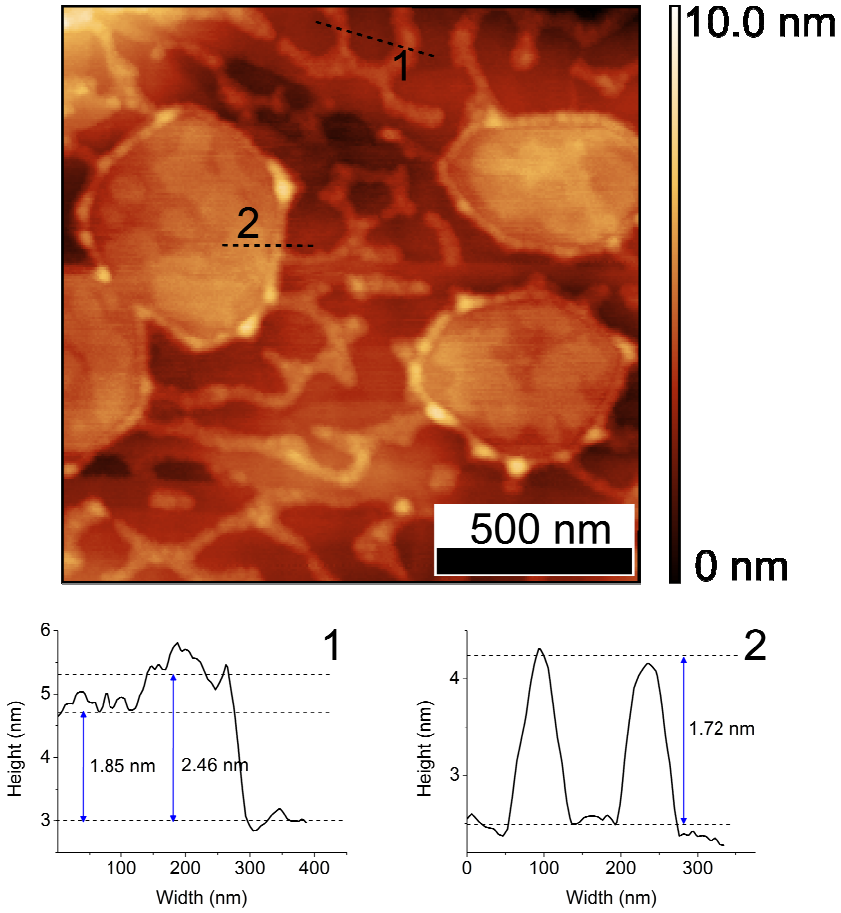

Figure 14. Top: 1.5×1.5 µm topographical AFM image of a 15% mix of PCBM in DH6T on HOPG. The image shows features of islands and ridges covering the HOPG. The graphs on the bottom correlate with the two cross sections marked in the top image. Each cross section shows an island height range of 1.85 nm to 2.46 nm and a ridge height of ~1.72 nm.

There were many new features seen on this film. A new island feature was present. Although these new islands had a higher perimeter along their edges, the internal height of the island at 1.85 nm was similar to the height of the island in the DH6T film. There were small height fluctuations along the top surface of the island. The ridges around the islands branched out across the microgram like a spider web, but they did not cross any island. These ridges had a consistent height averaging 1.72 nm. When looking farther out at the sample, such as Figure 15, we see more variety of the features.

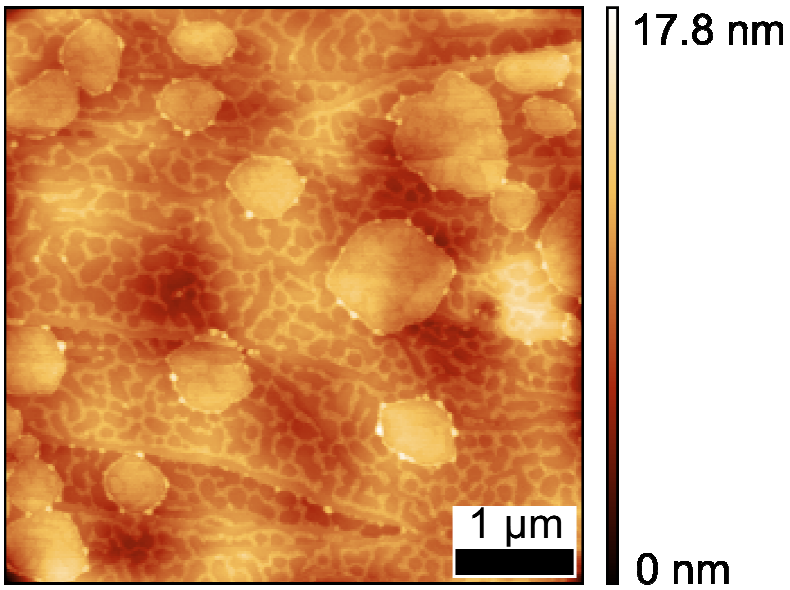

Figure 15. 5x5 µm topographical AFM image of a 15% mix of PCBM in DH6T on HOPG. This micrograph is a zoomed out image of Figure 14. The image shows more islands and ridges over HOPG. There are more islands of varying sizes with a uniform coverage of ridges.

There were an apparent variety of sizes of the islands at a larger scan size. A boundary around the islands that was higher than the inside of the flat surface of the island was also visible in the larger micrograph. Some islands had diameters up to one µm. It was also easier to see the HOPG features in the background, such as the wavy surface and step edges. The ridges tended to collimate at the edge of the steps on the graphite and spread across the flat graphite in a web like formation throughout the film. This mixture film was further explored through Kelvin Probe Force Microscopy (KPFM) in Figure 16.

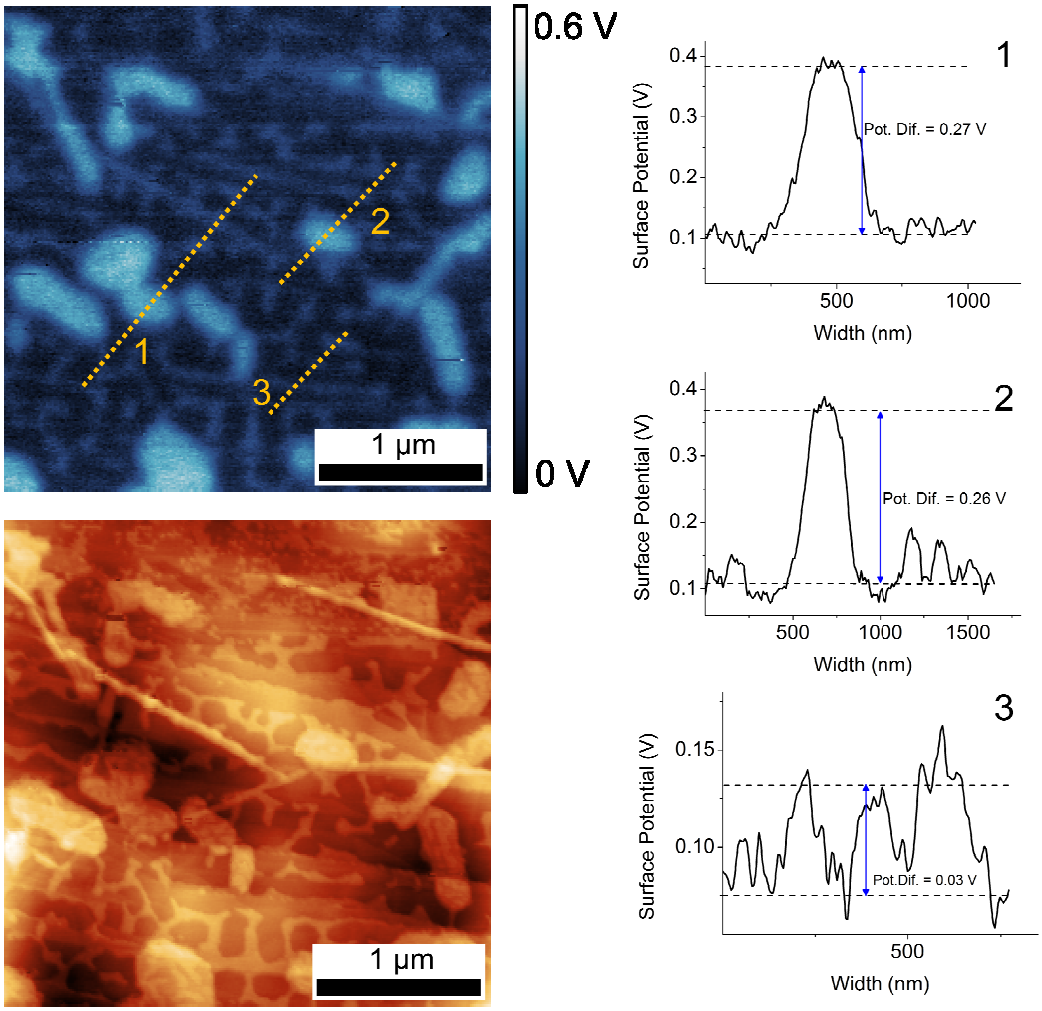

Figure 16. Top left panel is a 3×3 µm surface potential KPFM image of a 15% mix of PCBM in DH6T on HOPG. The lighter features correspond to the islands with a potential difference of 0.26 and 0.27 V, and the darker blue and black correspond to the ridges with a surface potential of 0.03 V. Bottom left is the matching topographic image. The right panels are the cross-section profiles as marked in the KPFM image.

In this study, the KPFM was used to compare surface potential difference between surface features. The top left KPFM microgram was displayed in a blue color map to distinguish KPFM from topographical AFM data. The island features showed the highest surface potentials in the KPFM microgram. On the right of Figure 16, cross sections 1, 2, and 3 show the surface potential profiles as marked in the KPFM image. The cross-sections 1 and 2 indicate the surface potentials of the island features were 0.26 – 0.27 V higher than that of the substrates, while the cross-section 3 showed that the

surface potential of the ridge features was only about 0.03 V higher. These surface potential value differences are consistent across the image, suggesting that the island features were intrinsically different from the ridge features. It is known that the work function of DH6T is less than that of PCBM, with DH6T having a work function of 3.94 eV, PCBM having a work function of 4.37 eV, and a blend of PCBM and DH6T was reported to have a work function of 4.06 eV.[40] Therefore, pure DH6T features were expected to display higher surface potential values than pure PCBM features. The surface potentials of their mixtures were likely to have a value between the two pure compounds. We speculated that the islands would have a higher concentration of DH6T than the ridge features. On the other hand, it had been shown that the surface potentials of surface features are also significantly impacted by their local morphologies, molecular arrangements, and local environments.[28]

To better understand the molecular packing of DH6T and PCBM and their intermolecular interactions, a molecular packing modeling was also carried out using Spartan 10. A C_{60} fullerene molecule was used instead of PCBM to simplify the calculation. The energy-minimized configuration of a DH6T and a C_{60} on a sheet of graphene is shown in Figure 17.

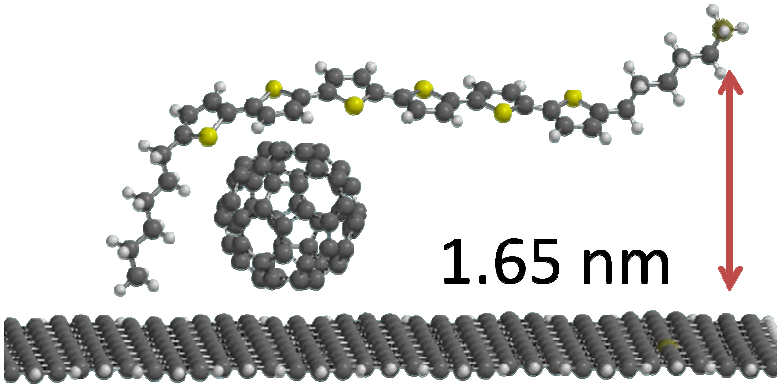

Figure 17. A scheme of one DH6T and one fullerene on a graphene layer, the configuration is energy-optimized with Spartan 10. The height is 1.65 nm.

As discussed earlier, an isolated DH6T molecule tends to stretch out and maintain its straight rigid backbone. The interaction from a fullerene molecule attracted the DH6T and forced the sexithiophene backbone to contour around the fullerene, as displayed in Figure 17. This was likely due to the π–π interactions between the thiophene rings and the conjugated carbon rings on fullerene. This configuration yielded a height of 1.65 nm that is very close to the measured height (~1.7 nm) of the island features in Figure 14. Although this model is just a crude attempt to re-construct the molecular arrangements of the BOFT, it did demonstrate that intermolecular interactions between DH6T and fullerene molecules were strong enough to bend the thiophene backbones and lead to surface features whose heights were very different from the height of pure DH6T.

30% Mixture

A 30% PCBM in DH6T solution in chlorobenzene had a PCBM concentration of 3.0×10^{-4} M and a DH6T concentration of 9.8 x 10^{-4} M. This mixture was spin-casted on an HOPG substrate and imaged as seen in Figure 18.

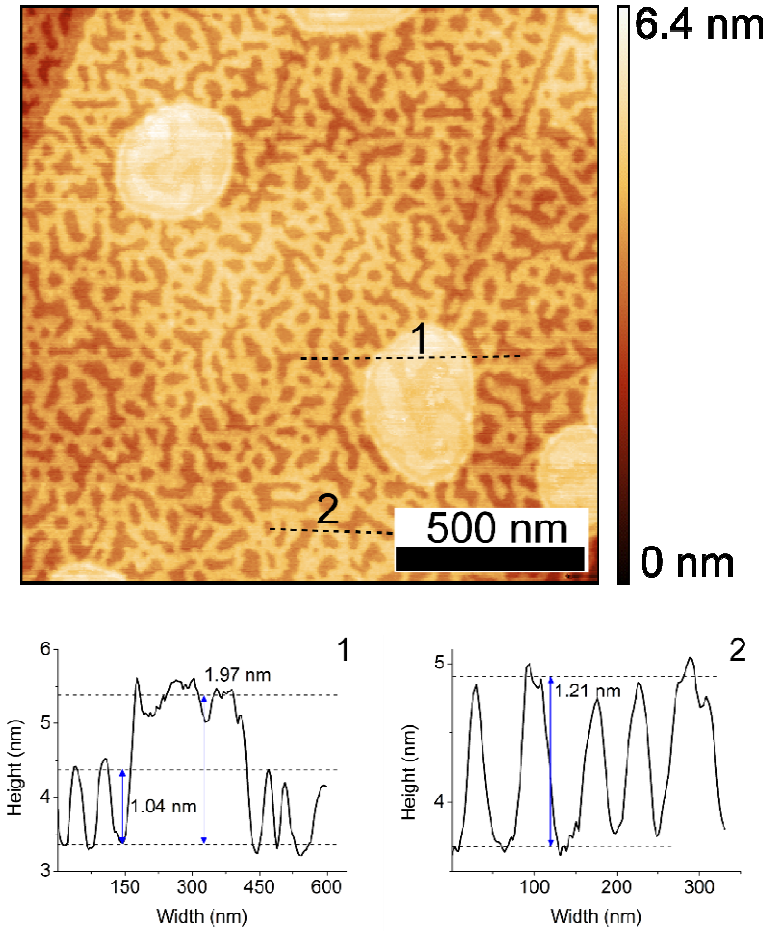

Figure 18. Top: 1.5×1.5 µm topographical AFM image of a 30% mix of PCBM in DH6T on HOPG. The image shows islands and ridges covering HOPG. Bottom: two cross sections correlate to the marked lines in the top AFM image. Each cross section shows an island height range of ~ 1.97 nm and a ridge height range of ~ 1.04 nm to1.21 nm.

The microgram showed similar features to Figure 14. The islands were also seen in this particular piece of data with a higher perimeter along their edges. The higher perimeter shown was thinner and less noticeable than the perimeter of the islands in 15%

mixture thin film. In this film, the cross section 1 of the island features corresponded to a height of ~1.97 nm with small height fluctuations. Similar to the spider web branching of the ridges seen in the 15% thin film, the ridges seen in Figure 18 were tightly packed and do not cross any island. From cross-sections 1 and 2, the ridge heights were measured to be 1.04 to 1.21 nm. A larger scale image of this mix can be seen in Figure 19.

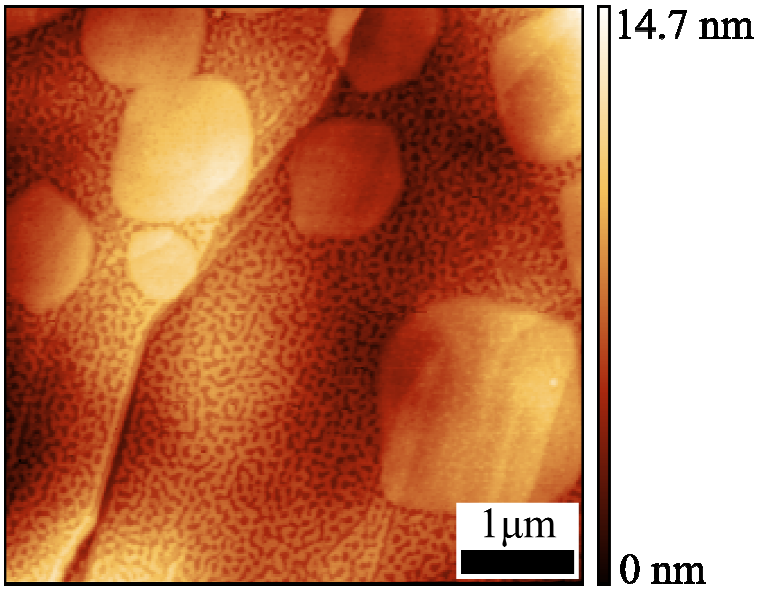

Figure 19. 5x5 µm topographical AFM image of a 30% mix of PCBM in DH6T on HOPG.

At a larger scan size, a wider variety of island sizes could be viewed. Some of the island diameters were greater than 1 µm. Step edges were clearly visible in Figure 19. The web of ridges was covering the entire remaining surface while collimated at the step edges on graphite. The 30% mixture ridges packed closer compared to the ridges in the 15% PCBM/DH6T mixture film. Some islands laid over step edges instead of stopping on a step edge. A KPFM scan of the same area was taken and the data was analyzed in Figure *20* to show the different features' surface potentials.

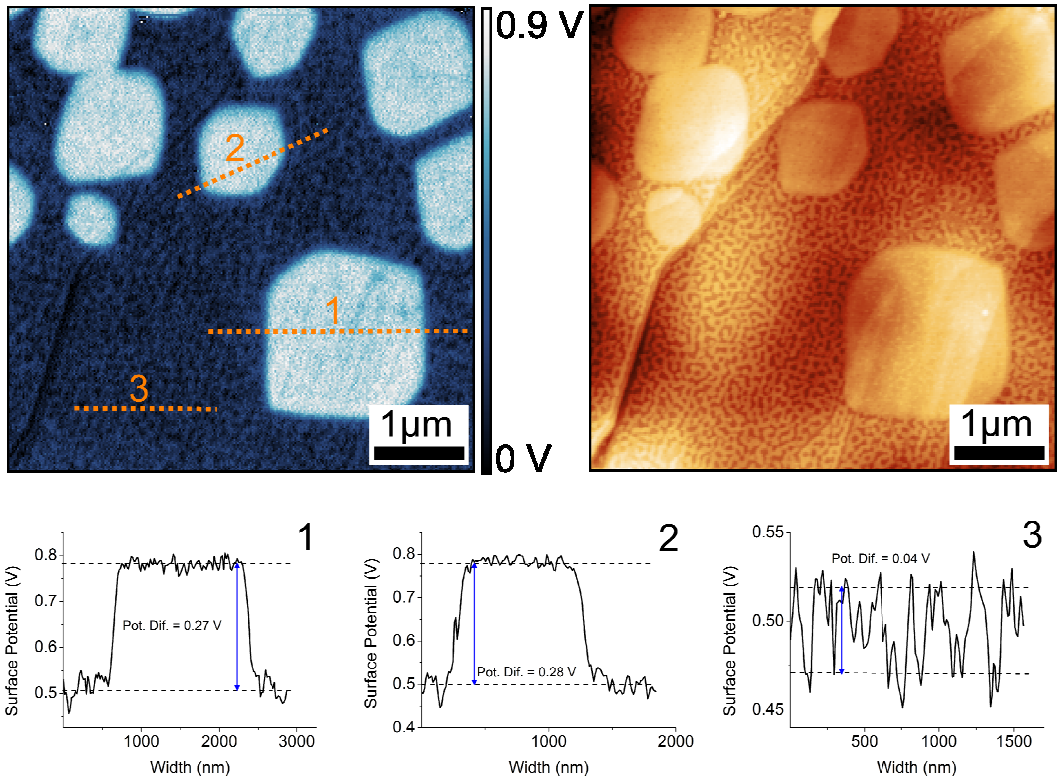

Figure 20. 3×3 µm surface potential KPFM image of a 30% mix of PCBM in DH6T on HOPG. The lighter features correspond to the islands with a potential difference of 0.27 V, and the darker blue and black correspond to the ridges with a surface potential of 0.04 V.

To the left in

Figure *20*, the KPFM microgram in blue shows a variety of surface potentials on the film. The lightest features shown are the islands with highest surface potentials. The surface potential of the islands are not affected by the step edges, unlike the topographical islands having a variety of heights due to the height change of the underneath substrate. This clearly demonstrates the selectivity of the KPFM measurement on the surface electronic properties over topographic properties. On the bottom of

Figure *20*, cross sections 1, 2, and 3 showed the surface potential profiles as marked in the KPFM image. From cross sections 1 and 2, the potential difference between the islands and the substrate were 0.27 V and 0.28 V, respectively. The ridge's

potential, shown in cross section 3, was 0.04 V higher than that of the substrate, which is smaller in comparison to the islands' values. These values suggested that the island features were probably electronically different from the ridge features. In relation to the ridge features in the 15% mixture film, the potential difference of ridges in the 30% mixture was similar. The islands will probably have a higher ratio of DH6T molecules than the ridges, resulting in higher surface potentials. As the PCBM ratio was increased from 15% to 30%, a model was made to explain possible molecular arrangements in the island features, as displayed in Figure 21.

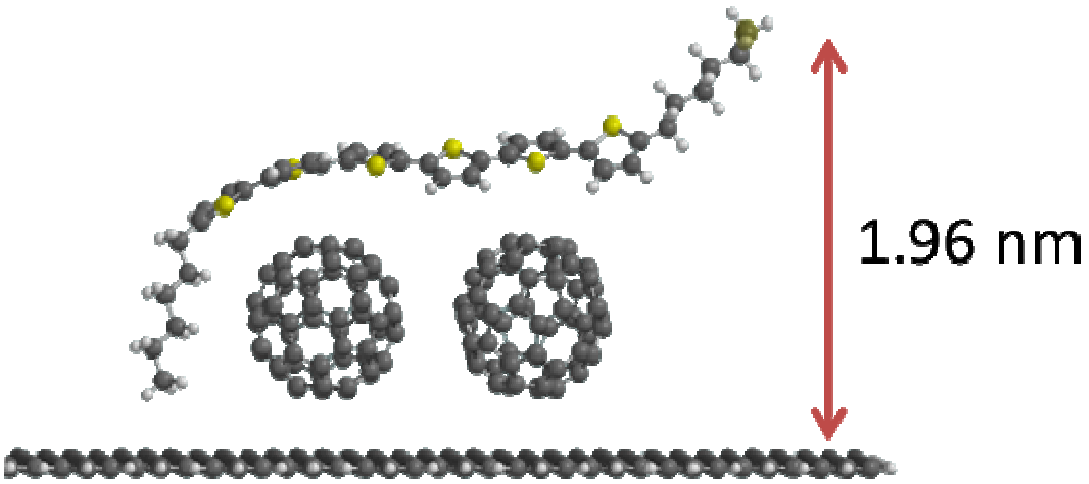

Figure 21. A scheme of one DH6T and two fullerene modeled with Spartan 10. The height was 1.96 nm.

The scheme in Figure 21 incorporated another fullerene to see how the DH6T will respond to the extra fullerene compared with the previous model of one DH6T and one PCBM. The DH6T was pulled down by both fullerenes' intermolecular π-π interactions with its sexithiophene backbone. In the 30% mixture film, the ridge features tended to be around 1 nm high, which were very close to the size of PCBM and fullerene. DH6T can also possibly align horizontally on the graphite surface. Figure 22 is a possible

representation of how the ridges could be formed. The scheme shown in Figure 22 showed two DH6T with a fullerene trapped between them. DH6T molecules could lie flat on the graphene surface due to the π–π interactions between its sexithiophene backbone and the conjugated carbon rings of graphene. The topographic height given by this model was 1.02 nm. Fullerenes were possibly trapped within fallen DH6Ts, leading to the low heights of ridge features observed in the 15% and the 30% PCBM in DH6T films.

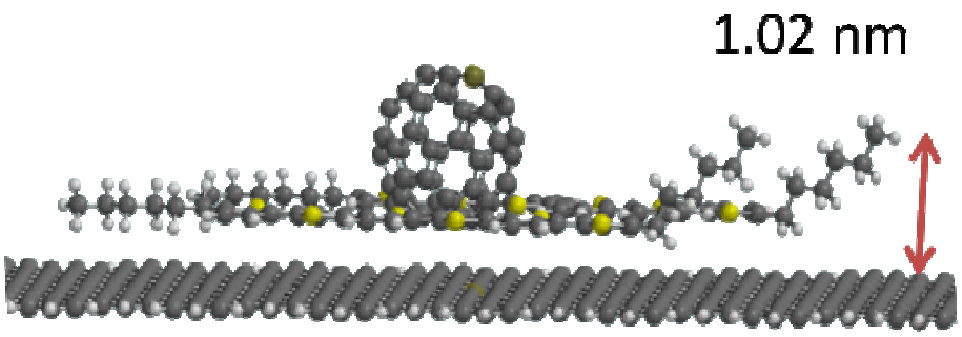

Figure 22. A scheme of two DH6T and one fullerene modeled with Spartan 10. The height is 1.02 nm.

50% Mixture

A 50% PCBM in DH6T solution in chlorobenzene had a PCBM concentration of 5.0×10^{-4} M and a DH6T concentration of 9.8×10^{-4} M. This mixture was spin-casted on an HOPG substrate and the AFM image of the resulting film is shown in Figure 23.

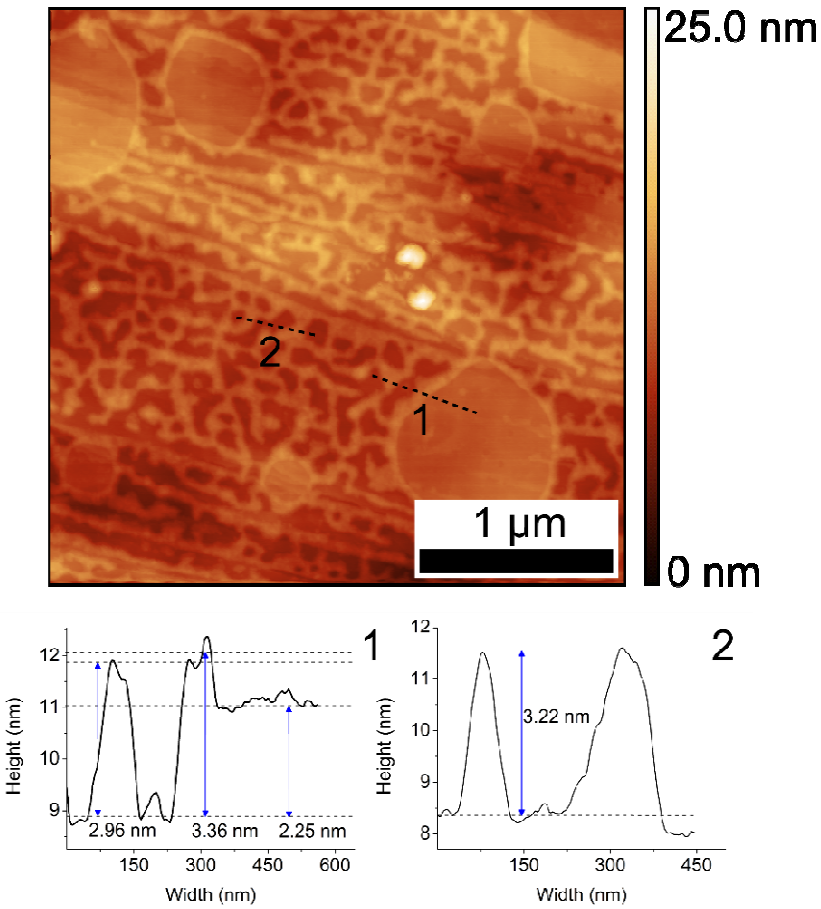

Figure 23. Top: 3×3 µm topographical AFM image of a 50% mix of PCBM in DH6T on HOPG. Bottom: two cross-sections correlate to the marked lines in the AFM image. Each cross-section shows an island height range of 2.25 nm to 3.36 nm and a range of ridge heights from 2.96 nm to 3.22 nm.

In the 50% mixture film shown in Figure 23, the islands have different sizes and were scattered throughout the image just like the previous mixture films. The ridges were dispersed evenly throughout the substrate and were similar to the ridges in the 30% mixture. A smaller scale image was taken to further observe the island feature and its rough surface, as seen in Figure 24. When Figure 24 was first scanned, it was questionable whether there was a fault in the scan, or this feature was unique. By scanning other areas, the roughness on top of the island was consistently seen multiple times. One of the other areas shown in Figure 25 that had the same size as the Figure 24

with a dimension of 1.5×1.5 µm. Figure 25 showed four smaller islands in comparison to one large island in Figure 24. The four islands in Figure 25 still show a rough topography surface demonstrating that these features are very likely real.

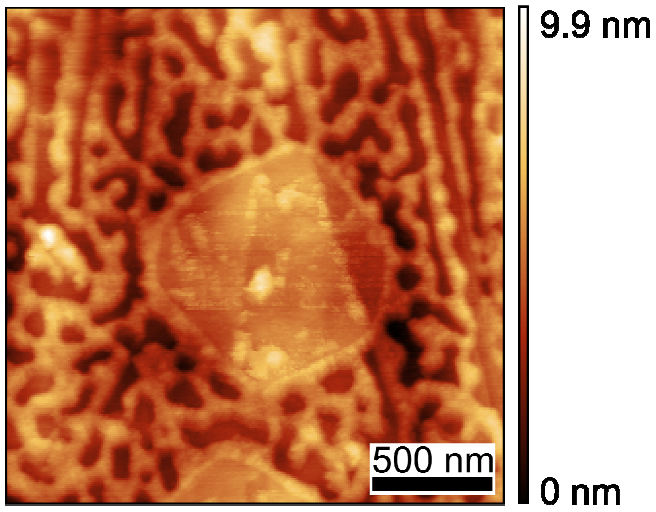

Figure 24. 1.5×1.5 µm topographical AFM image of a 50% mix of PCBM in DH6T on HOPG.

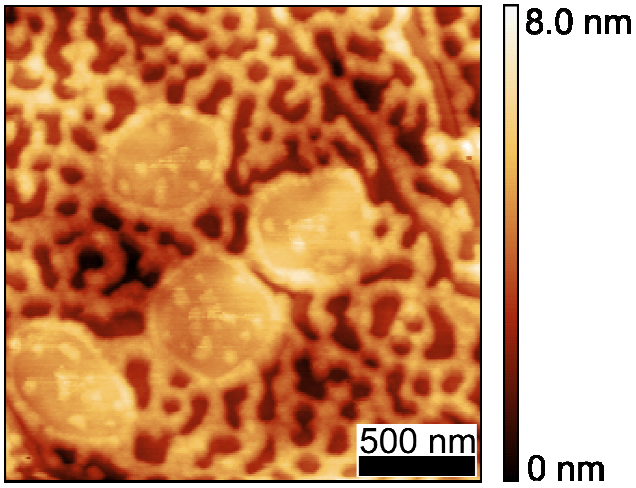

Figure 25. 1.5×1.5 µm topographical AFM image of a 50% mix of PCBM in DH6T on HOPG. This image is a close up of the 50% mixture of PCBM and DH6T on HOPG.

A KPFM study was conducted for 50% mixture film, as shown in Figure 26. These islands can be seen as the lighter blue features in the KPFM microgram. The surface potential differences between the islands and the substrate ranged from 0.29 V to

0.31 V, which were very similar to both 15% and 30% mixture films. Unlike the other ridge features in the previous 15% and 30% mixes, the potential difference between the ridge features and the substrate in the 50% mixture film was about 0.07 V, sometimes larger than 0.10 V. As shown in Figure 23, the ridge features have topographic heights of 3.2 nm, much higher than that in both 15% and 30% mixture films. This change in the height and potential difference of the ridges in the 50% mixture film suggested a change in either their composition or molecular arrangements.

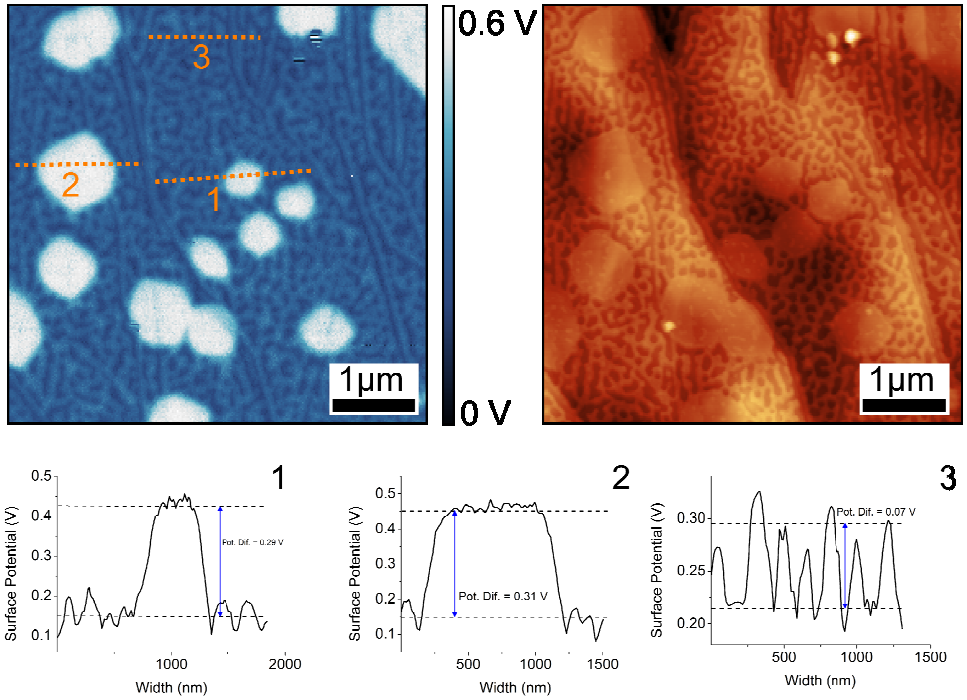

Figure 26. Top left is 5×5 μm surface potential KPFM image of a 50% mix of PCBM in DH6T on HOPG. Top right is the matching AFM image. The bottom panels are the cross-section profiles as marked in the KPFM image.

The 5×5 μm topographic scan seen in the top right panel of Figure 26 showed that the island height in the 50% mixture film was consistent with the other mixture films. Similarities in height and surface potentials of the island features in the 50% mixture film to that of the 30% and 50% films indicated that the island features in all three films had almost the same molecular packing. With the height variations for the ridges, theoretical

modelings were employed to give possible configurations of the molecules on the surface of graphite, as seen in Figure 27. The arrangement of three DH6T and two fullerene molecules were attempted on the surface. Sandwiched by the two fullerene molecules, the DH6T molecules may pack and adopt a standing-up geometry. It should be noted that this scheme was only a possible explanation of the higher ridges. The increase of PCBM concentration may give a higher ridge feature by the DH6T molecules being pushed upright between the PCBMs. Also, since the surface potential of the ridges was slightly higher in the 50% film than that in the 30% and the 15% mixture films, there was a possibility that the upright geometry of DH6T could lead to slightly elevated surface potential values.

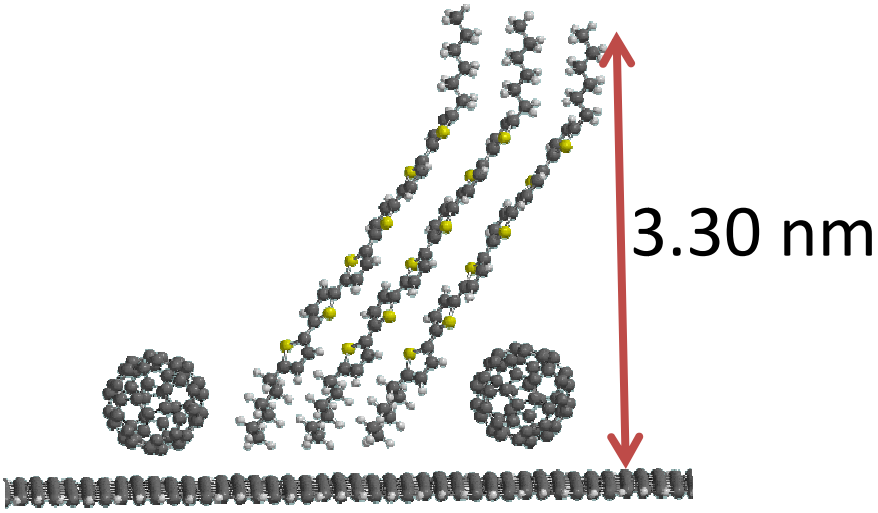

Figure 27. A scheme of three DH6T and two fullerene modeled with Spartan 10. The height is 3.30 nm.

Annealing Studies

The mixture films prepared by spin-casting often ended up in a kinetically trapped state. Annealing, especially thermal solvent annealing, could rearrange the molecules in the films into a more thermodynamically stable state. In this section, both the spin-casted 15% and 30% mixture films were thermal solvent annealed. Annealing was done by placing a substrate with the mixture film in a container that also contained a well of chloroform. This container was sealed and set in a 65^{o}C oven for annealing.

After the annealing for 12 hours, a KPFM with a coordinating topography scan of the 15% mixture film was taken as seen in Figure 28. In the annealed 15% sample, the step edge and waviness of the graphite surface was visible and the islands were well defined. The potential difference between these islands and the substrate was 0.28 V, which was similar to the potential difference before annealing. The ridge features were not connecting as well as they did in the non-annealed 15%. The center of the island features appeared to have rough surfaces similar to the islands in the 50% spin-casted films.

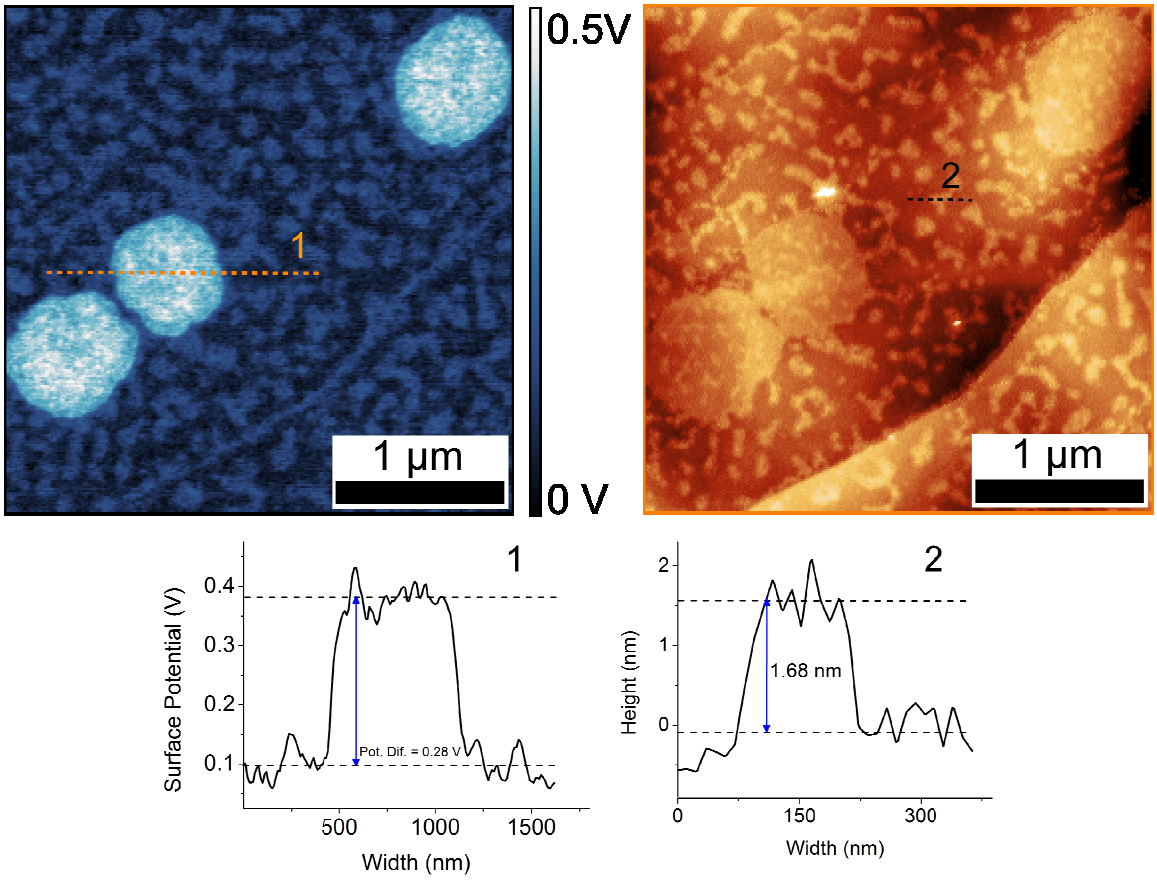

Figure 28. A 3×3 µm KPFM image (top left) and matching topography microgram (top right) of the 15% mixture film after annealing. The bottom panels are the cross-section profiles as marked in the top images.

Annealing the 30% mixture was next, as seen in Figure 29. The top right topographic image had many step edges. The biggest differences resulting from the annealing process was that there were no more round island features and the ridge features were totally missing. In the KPFM image, there were mainly two kinds of areas, the lighter one and the darker one. The potential difference from the lighter KPFM area to the darker KPFM area was 0.08 V, which was close to the potential difference between the ridges and the substrate in the 50% mix sample. It was possible that the darker area were composed of PCBM molecules that push the DH6T molecules to pack into upright

islands, which showed a higher surface potential value and lighter color in the KPFM image.

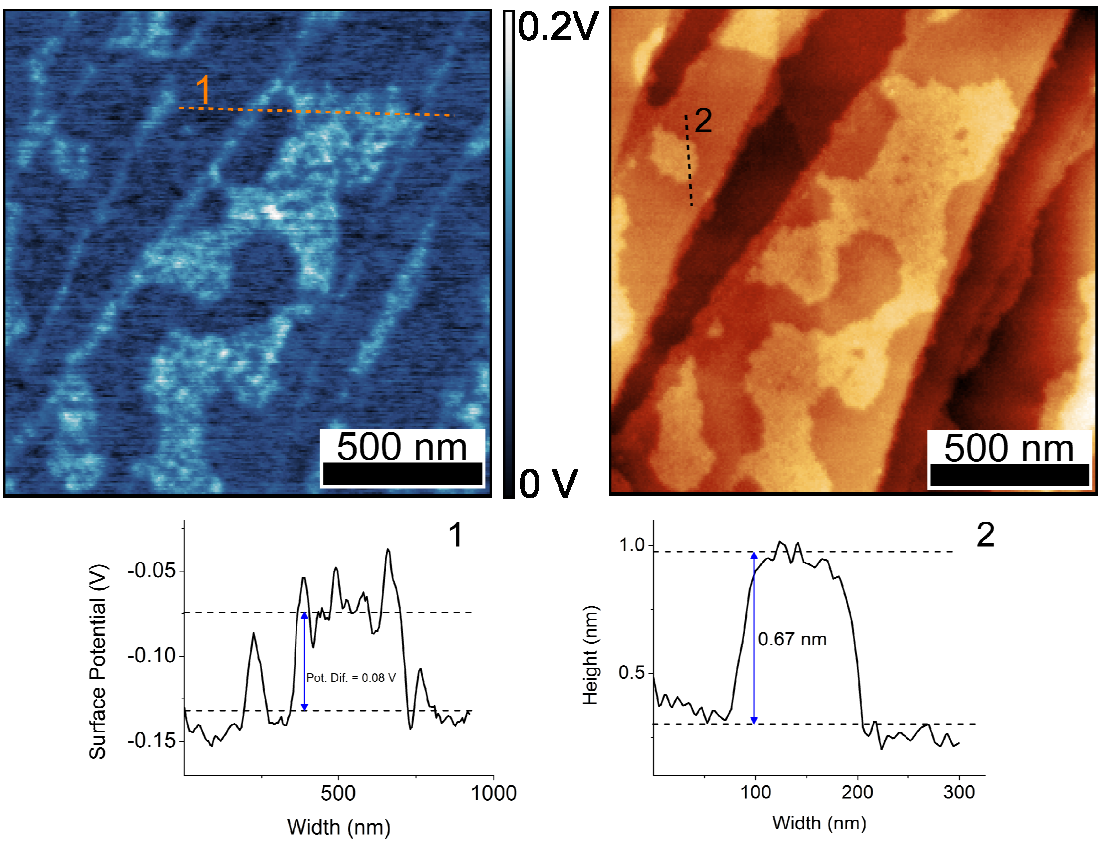

Figure 29. Top left: a 1.5×1.5 KPFM image with a matching topography microgram after annealing. Top right: matching topography microgram. The bottom panels are the cross-section profiles as marked in the top images.

CHAPTER V

CONCLUSION

Findings and Significance

A concentrated DH6T solution in chlorobenzene spin-casted on HOPG showed monolayer thick island-like features scattered throughout the substrate. These islands were explained in an upright-packing model using Spartan that agreed with the experimental results. These results also were consistent with previous literature on the number of thiophene oligomer molecules in relation to their packing orientation.[8] Theoretical modeling also supported that DH6T molecules tend to order in a staggered manner due to π-π interactions. It was also observed that PCBM had a greater affinity to the HOPG, resulting in a full coverage of PCBM on the substrate with pits scattered throughout the film. The AFM and KPFM results of these films were summarized in Table 1. After mixing PCBM and DH6T to form a 15% mixture film on HOPG, the addition of PCBM added ridge features that had surface potential values closer to pure PCBM in the KPFM analysis. The island features observed in mixture films were topographically lower than the pure DH6T islands. It was likely due to the strong attraction from the PCBM that altered the packing angle and geometry of DH6T, lowering the island topographic heights. Again with the 30% mixture, the island features showed similar height and surface potential values as the islands observed in the 15% mixture. The ridges seemed to be very similar to PCBM in terms of both height and surface potential. For the 50% mixture, the ridges and the perimeter of the islands were much higher but had a lower surface potential, which could possibly be explained by a multilayer of PCBM mixed with a small amount of DH6T. The fullerenes could push up

DH6T to make them stand upright, yielding a higher topographic height. With this added amount of PCBM the inner island was topographically higher than the previous mixtures also. The KPFM surface potentials of the islands matched with the other mixture's surface potential, the surface potential of the ridges was much lower than the other ridges in the 15% and 30% mixtures.

Table 1

Summary of heights and surface potentials measured for pure DH6T, pure PCBM, and their mixture films on HOPG.

	Height (nm)			Surface potential (V)		
	Substrate	Ridges	Island	Substrate	Ridges	Island
Pure PCBM	0	1.15	x	x	x	x
Pure DH6T	0	x	2.6	x	x	x
15% Mixture	0	1.72	1.85	0	0.03	0.27
30% Mixture	0	1.21	1.97	0	0.04	0.28
50% Mixture	0	3.22	2.25	0	0.07	0.29

Future Directions

The study has shown morphologically that adding PCBM did have a dramatic impact on the packing of DH6T in a BOTF environment. With Kelvin Probe Force Microscopy, differentiating the phases of the film was possible. Some preliminary data of annealing experiments showed the 15% mixture's island surface potential was similar to that of the unannealed 15% and 30% mixtures. For future work, different annealing

conditions on varying ratio of PCBM to DH6T would be interesting to test. Also, a conductive AFM study would provide new insights on conductivity of different BOFTs, both before and after annealing.

REFERENCES

1. Mukherjee, B.; Mukherjee, M. Langmuir 2011, 27, 11246.

2. Ebenhoch, B.; Thomson, S. A. J.; Genevicius, K.; Juska, G.; Samuel, I. D. W. Organic Electronics 2015, 22, 62.

3. Chang, J. H.; Lin, W. H.; Wang, P. C.; Taur, J. I.; Ku, T. A.; Chen, W. T.; Yan, S. J.; Wu, C. I. Scientific Reports 2015, 5, 6.

4. Waldauf, C.; Schilinsky, P.; Perisutti, M.; Hauch, J.; Brabec, C. J. Adv. Mater. (Weinheim, Ger.) 2003, 15, 2084.

5. Chang, P. C.; Lee, J.; Huang, D.; Subramanian, V.; Murphy, A. R.; Frechet, J. M. J. Chemistry of Materials 2004, 16, 4783.

6. Berriman, G.; Routley, B.; Holdsworth, J.; Zhou, X. J.; Belcher, W.; Dastoor, P. Measurement Science & Technology 2014, 25, 6.

7. Wang, Y.-T.; Chen, M.-H.; Lin, C.-T.; Fang, J.-J.; Chang, C.-J.; Luo, C.-W.; Yabushita, A.; Wu, K.-H.; Kobayashi, T. ACS Applied Materials & Interfaces 2015, 7, 4457.

8. Hlawacek, G.; Teichert, C. Journal of Physics-Condensed Matter 2013, 25.

9. Nuyken, O.; Jungermann, S.; Wiederhirn, V.; Bacher, E.; Meerholz, K. Monatshefte für Chemie / Chemical Monthly 2006, 137, 811.

10. Pagliaro, M.; Ciriminna, R.; Palmisano, G. ChemSusChem 2008, 1, 880.

11. Krebs, F. C. Sol. Energy Mater. Sol. Cells 2009, 93, 1636.

12. Coenen, M. J. J.; Slaats, T. M. W. L.; Eggenhuisen, T. M.; Groen, P. Thin Solid Films 2015, 583, 194.

13. Günes, S.; Neugebauer, H.; Sariciftci, N. S. Chemical Reviews 2007, 107, 1324.

14. Krebs, F. C. Sol. Energy Mater. Sol. Cells 2009, 93, 484.

15. Krebs, F. C. Solar Energy Materials and Solar Cells 2009, 93, 394.

16. Dang, M. T.; Hirsch, L.; Wantz, G.; Wuest, J. D. Chemical Reviews 2013, 113, 3734.

17. Young, T. J.; Monclus, M. A.; Burnett, T. L.; Broughton, W. R.; Ogin, S. L.; Smith, P. A. Measurement Science and Technology 2011, 22, 125703.

18. Yin, N.-N.; Buyanin, A.; Riechers, S. L.; Lee, O. P.; Frechet, J. M. J.; Salmeron, M.; Liu, G.-y. Journal of Physical Chemistry C 2014, 118, 5789.

19. Radziwon, M.; Madsen, M.; Balzer, F.; Resel, R.; Rubahn, H.-G. Thin Solid Films 2014, 558, 165.

20. Mannebach, E. M.; Spalenka, J. W.; Johnson, P. S.; Cai, Z. H.; Himpsel, F. J.; Evans, P. G. Advanced Functional Materials 2013, 23, 554.

21. Murphy, A. R.; Frechet, J. M. J.; Chang, P.; Lee, J.; Subramanian, V. Journal of the American Chemical Society 2004, 126, 1596.

22. Wang, L.; Ye, S. H.; Yuan, H. Z.; Song, Y. H.; Zhu, H. Z.; Hou, H. Q.; Li, P. C. Microscopy and Microanalysis 2012, 18, 844.

23. Duhm, S.; Salzmann, I.; Koch, N.; Fukagawa, H.; Kataoka, T.; Hosoumi, S.; Nebashi, K.; Kera, S.; Ueno, N. Journal of Applied Physics 2008, 104.

24. Spoltore, D.; Vangerven, T.; Verstappen, P.; Piersimoni, F.; Bertho, S.; Vandewal, K.; Van den Brande, N.; Defour, M.; Van Mele, B.; De Sio, A.; Parisi, J.; Lutsen, L.; Vanderzande, D.; Maes, W.; Manca, J. V. Organic Electronics 2015, 21, 160.

25. Gao, H. L.; Zhang, X. W.; Meng, J. H.; Yin, Z. G.; Zhang, L. Q.; Wu, J. L.; Liu, X. Thin Solid Films 2015, 576, 81.

26. Murphy, A. R.; Frechet, J. M. J. Chemical Reviews 2007, 107, 1066.

27. Mishra, A.; Ma, C.-Q.; Baeuerle, P. Chemical Reviews 2009, 109, 1141.

28. Ouhib, F.; Tomassetti, M.; Manca, J.; Piersimoni, F.; Spoltore, D.; Bertho, S.; Moons, H.; Lazzaroni, R.; Desbief, S.; Jerome, C.; Detrembleur, C. Macromolecules 2013, 46, 785.

29. D'Avino, G.; Muccioli, L.; Zannoni, C. Advanced Functional Materials 2015, 25, 1985.

30. Hauch, J. A.; Schilinsky, P.; Choulis, S. A.; Childers, R.; Biele, M.; Brabec, C. J. Solar Energy Materials and Solar Cells 2008, 92, 727.

31. Gutierrez-Gonzalez, I.; Molina-Brito, B.; Gotz, A. W.; Castillo-Alvarado, F. L.; Rodriguez, J. I. Chemical Physics Letters 2014, 612, 234.

32. Korona, T.; Rutkowska-Zbik, D. Computational and Theoretical Chemistry 2014, 1040, 243.

33. Li, L. H.; Kontsevoi, O. Y.; Freeman, A. J. Journal of Physical Chemistry C 2014, 118, 10263.

34. Muhammad, F. F.; Sulaiman, K. Thin Solid Films 2011, 519, 5230.

35. Zotti, G.; Vercelli, B.; Berlin, A. Accounts of Chemical Research 2008, 41, 1098.

36. Duhm, S.; Xin, Q.; Koch, N.; Ueno, N.; Kera, S. Organic Electronics 2011, 12, 903.

37. Yamagata, H.; Pochas, C. M.; Spano, F. C. Journal of Physical Chemistry B 2012, 116, 14494.

38. Paterno, G.; Warren, A. J.; Spencer, J.; Evans, G.; Sakai, V. G.; Blumberger, J.; Cacialli, F. Journal of Materials Chemistry C 2013, 1, 5619.

39. Ruoff, R. S.; Hickman, A. P. The Journal of Physical Chemistry 1993, 97, 2494.

40. Maibach, J.; Mankel, E.; Mayer, T.; Jaegermann, W. Surface Science 2013, 612, L9.